ChemComm

Cubic SnGe Nanoalloys: Beyond Thermodynamic Composition Limit

Journal:	*ChemComm*
Manuscript ID	CC-COM-09-2018-007570.R1
Article Type:	Communication

Journal Name

COMMUNICATION

Cubic SnGe Nanoalloys: Beyond Thermodynamic Composition Limit

Received 00th January 20xx,
Accepted 00th January 20xx

DOI: 10.1039/x0xx00000x

www.rsc.org/

Karthik Ramasamy,*[a] Paul G. Kotula,[b] Norman Modine,[b] Michael T. Brumbach,[b] Jeffrey M. Pietryga,[c] Sergei A. Ivanov*[a]

Tin-germanium alloys are increasingly of interest as optoelectronic and thermoelectric materials as well as materials for ion battery electrodes. However, the lattice incompatibility of bulk Sn and Ge makes creating such alloys challenging. Exploiting the unique strain tolerance behavior of nanosized crystals, we have deveoped a facile synthesis method for homogeneous, Sn_xGe_{1-x} alloy nanocrystals with composition varied from essentially pure Ge to 95% Sn while still maintaining the cubic structure.

Due to favorable electronic properties[1,2] and its low-cost and compatibility with existing CMOS processing methods, germanium (Ge) has found applications in many electronic and optoelectronic devices.[3-6] More recently, it has also been studied as an anode for Li and Na ion batteries.[7,8] However, bulk Ge's inherently inefficient light absorption/emission and large volume changes during lithiation/delithiation have hindered its use in such applications.[9,10] Alloying of Ge with Sn can potentially address both issues;[11-20] however, the low solubility (< 1% of Sn in Ge) and large lattice mismatch between Ge and Sn[21] means that achieving a significant degree of alloying requires elaborate "lattice engineering." For instance, thin films of Sn_xGe_{1-x} alloy with Sn content up to 26% have been sandwiched between two Ge layers via MBE.[22] In addition, the use of Ge/Si(001)-virtual substrates has allowed deposition of thin alloy films with up to 13% Sn that exhibit low temperature fluorescence and lasing,[17] implying at least a partial indirect-to-direct gap transition that would open the door to a range of near-infrared (near-IR) light absorbing/emitting applications. Unfortunately, such films are expensive to produce at large scale, and have band gaps too narrow for, e.g., solar energy conversion applications.

In contrast, we have previously shown that free standing Sn_xGe_{1-x} ($0 \le x \le 0.42$) alloy NCs, with wider optical band gaps due to quantum confinement effects, can be produced efficiently by colloidal synthesis.[23] However, neither this nor related efforts[24-29] produced distinctive evidence for the predicted indirect-to-direct gap transition, implying still larger Sn-content is needed to achieve this transition in quantum-confined alloy NCs. As an enabling step in this investigation, here, we report the synthesis of cubic Sn_xGe_{1-x} NCs over essentially the complete compositional range of $0 \le x \le 0.95$. Further, we describe a simple method for controlled surface sulfidization of alloy NCs that increases their thermal stability up to 500 °C while also rendering them amenable to facile ligand exchange, critical characteristics for subsequent inclusion in electronic devices.

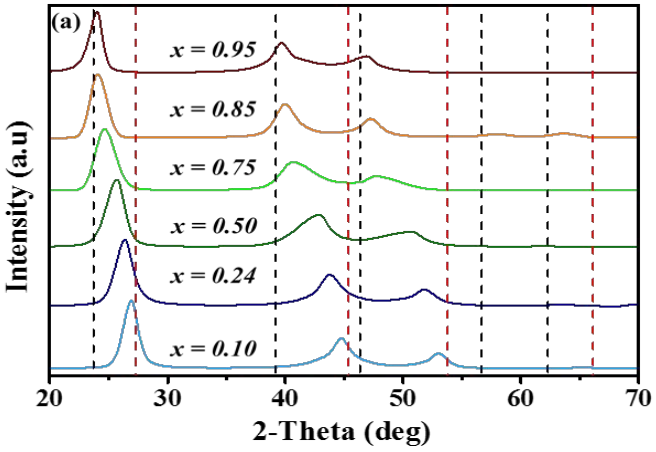

Fig 1. XRD patterns of Sn_xGe_{1-x} NCs with x between 0.10 and 0.95. Red and black dotted lines correspond to positions of diffraction lines of pure cubic Ge and α-Sn, respectively.

Synthesis of Sn_xGe_{1-x} NCs is accomplished by the reduction of controlled amounts of $Sn(amide)_2$ and GeI_2 by *n*-BuLi in alkylamine solution (see details in SI). XRD analysis reveals that the NCs retain the cubic crystal phase as the peaks shift toward lower 2θ with increased Sn content (Fig. 1), corresponding to a change in lattice constant from 5.65 Å for pure Ge NCs, to 6.44 Å for NCs with the highest Sn content. Using a previous study of bulk Sn_xGe_{1-x} alloy,[30] we extract the Sn fraction, *x*, from each sample, and find excellent agreement with values obtained from EDX and ICP measurements (Table S1). From TEM and SAXS measurements, average NC size is found to range from 7 nm to 16 nm, depending on reaction temperature and duration (Fig S1). The homogeneous distribution of

[a] Center for Integrated Nanotechnologies
Los Alamos National Laboratory
P. O. Box 1663, Los Alamos, New Mexico 87545 (USA)
E-mail: karthik@ubiqd.com; ivanov@lanl.gov
[b] Sandia National Laboratory
Albuquerque, New Mexico 87185 (USA)
[c] Center for Advanced Solar Photophysics
Los Alamos National Laboratory
P.O. Box 1662, Los Alamos, New Mexico 87545 (USA)

† Footnotes relating to the title and/or authors should appear here.
Electronic Supplementary Information (ESI) available: [details of any supplementary information available should be included here]. See DOI: 10.1039/x0xx00000x

elements within each alloy NC was verified by High Angle Annular Dark Field (HAADF) imaging combined with 2D EDX elemental mapping [shown in Fig 2(d-f) for $Sn_{0.75}Ge_{0.25}$ NCs] by applying a multivariate statistical analysis on the STEM-EDX mapping images.[23]

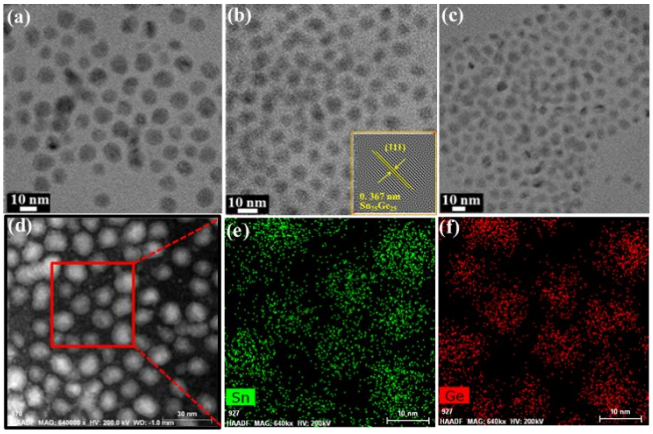

Fig 2. TEM images of Sn_xGe_{1-x} NCs (x = 0.50 (a), 0.75 (b) and 0.85 (c)) Inset: Inverse FFT of HRTEM image. (d) HAADF image of Sn_xGe_{1-x} NCs (x = 0.75. Sn (e) and Ge (f) STEM-EDX element mapping from the boxed area in panel (d).

Combined results from XRD, HAADF and STEM-EDX measurements allow us to rule out the homogenous nucleation of individual Sn and Ge nanoparticles as well as the formation of germanium islands (clusters) or a shell over the tin core down to sub-nm scale (see Fig S2 for higher magnification images).

While tuning the composition of an alloy of miscible constituents is typically effected by varying the ratio of corresponding reaction precursors,[31] for alloys of largely immiscible elements like Ge and Sn, we found this method not fully effective. For instance, when the ratio of $Sn(HMDS)_2$ to GeI_2 decreases from 1:1 to 1:2, x in the final product decreases only from 0.5 to 0.37, and chemical yield of the final product is reduced; further decrease in the Sn/Ge ratio to 1:3 did not yield any identifiable product at all. In contrast, reactions with Sn/Ge ratios above 1.25:1 predominantly yield tetragonal tin NCs. Thus, direct control over Sn-content in phase-pure NCs is afforded only over the narrow interval between 1.25:1 and 0.4:1 (Fig S3). Instead, we found control over reaction *temperature* and the *duration* of particle growth to be more effective ways to influence the NC composition. Fig S3 implies that at a 1:1 ratio of Sn:Ge precursors, the particle composition is the most sensitive to the reaction temperature, which in turn suggests NC formation may proceed via initial formation of a Sn-rich complex. A ^{119}Sn NMR study revealed (Fig S4) that the dissolution of $Sn(amide)_2$ in oleylamine first leads to formation of cubane $Sn_4(C_{18}H_{35}N)_4$ clusters.[32] Upon introduction of GeI_2, the corresponding resonance at 644ppm disappears and is replaced by a new resonance at 260-300ppm (Scheme 1), which likely indicates partial metal exchange in the cluster framework to form a mixed Sn/Ge complex. From these experiments, we infer that formation of a cubic Sn-complex, followed by partial metal exchange, is a key step in the formation of Sn_xGe_{1-x} alloy NCs, as the ease of Ge exchange with Sn points to the strong affinity for Ge to interact with small Sn nuclei.

We have isolated Sn_xGe_{1-x} nanoalloy with varying tin content from 7 % to 95 % when *n*-BuLi was used as a reducing agent (Fig S6 & Table S2). Despite such a high tin content in $Sn_{0.95}Ge_{0.05}$ particles, they retain the cubic structure instead of adopting the structure of β-Sn, which is thermodynamically preferred in pure bulk above 13°C. Nevertheless, all NCs obtained by this method show instability toward phase separation above 200-210°C with the formation of β-Sn and Ge. Expectedly, the rate of phase separation increases with temperature, and, as such, the highest amount of tin in Sn_xGe_{1-x} alloy can only be achieved at the lowest possible temperature of synthesis (ca 210°C) and short growth times.

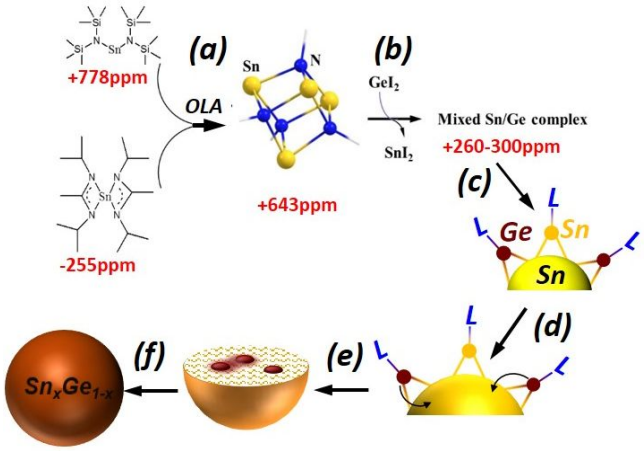

Scheme 1. Proposed pathway for the formation of Sn_xGe_{1-x} alloy NCs. ^{119}Sn{^{1}H} NMR chemical shifts are shown in red. The $C_{18}H_{35}$- chain of oleylamide is not shown for clarity. (***a***) Formation of tin cubane complex in OLA, (***b***) formation of Sn-Ge mix metal complex, (***c***) Reduction of tin and formation of Sn nanodroplets, (***d***) diffusion of Ge into Sn interior concomitant with the droplet growth, (***e***) formation of proeutectics (shaded area depicts the regidified regions of the alloy with lowered diffusion coefficient), (***f***) growth of the alloy particle as more Sn and Sn-Ge complexes decompose on the particle surface.

For example, NCs with x=0.95 were obtained at 210°C for 20 min of growth, but x decreases to 0.87 if growth is extended by another 10 min, and drops even more to 0.55 if NCs are grown for 60 min. The maximum x that can be achieved at 230°C was 0.75, which drops to 0.38 after an hour of growth. As it was also established, one cannot arbitrarily decrease the duration of the particle growth in order to obtain the product with higher tin content: if the growth duration is shorter than a threshold value (this value is a temperature dependent, *e.g.* 7-8 min at 210°C) the product unavoidably will contain small particles of pure β-Sn. Fig S7a presents the XRD data for products obtained at early stages of NCs growth at 210°C. Broad XRD pattern from the NCs isolated after 2 min can be assigned to tiny β-Sn NCs, which was further confirmed by matching the lattice distance of (220) plane observed on HRTEM image and reflections in the Small Area Electron Diffraction patterns (Fig S7b and c). The XRD pattern of the sample after 5 min of growth reveals the mixture of Sn-rich Sn_xGe_{1-x} alloy and β-Sn NCs. With further NC growth, only reflections corresponding to alloy NCs (with decreased tin content) are present, whereas those of β-Sn are no longer observed (Fig S7a). We believe that small β-Sn (<2 nm) particles are formed first at the early stages of the reaction, with Ge atoms being coordinated on the particle surface. At or above 200°C, β-Sn NCs are expected to be in a liquid phase due to their small size. The high chemical potential of germanium around the small nanodroplet of tin serves as a driving force for the diffusion of the former into the interior of the particle. As it follows from the Sn-Ge phase diagram, incorporation of even small amounts of Ge into Sn is likely to cause the formation of the proeutectic phase with higher melting point than that of pure Sn.

As such, germanium atoms effectively "rigidify" the local environment around them, kinetically trapping them in the particle interior. Simultaneously, the presence of Ge drastically increases the temperature for the α⇒β phase transition in tin, stabilizing the cubic phase of Sn_xGe_{1-x} alloy NCs (Scheme 1). Although the formation of the proeutectic phase slows the diffusion of Ge out of the nanocrystal, it does not stop the process.

As such, Sn-Ge phase separation – the thermodynamically preferred process – still occurs if given a sufficient combination of time and high temperature, leading to the depletion of tin in the final products.[33,34] Our preliminary DFT molecular dynamics (MD) simulations illustrate the viability of the proposed mechanism of the suppressed Sn-Ge phase separation in the produced nanoparticles (See SI for details).

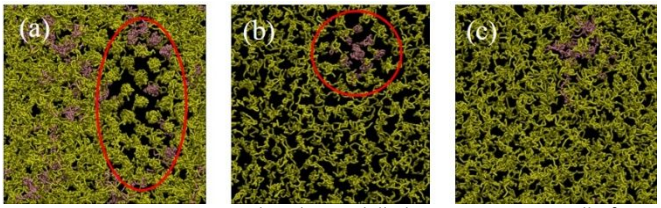

Fig 3. Atomic trajectories within the modelled 256 atom super-cell of SnGe alloy at 510K: (a) after 10ps of simulation with random distribution of 27 Ge atoms together with 5 clustered Ge atoms. (b) after 10ps of simulation with initial arrangement of 10 Ge atoms into a cluster with adamantane structure; (c) after 15ps of the same simulation as in (b). Red highlight emphasizes the appearance of crystalline regions within the molten alloy.

Fig 3a shows the atomic trajectories explored by the simulation at 510 K in which the initial 256-atom cell contained Sn except for 5 clustered and 27 randomly distributed Ge atoms (12.5% Ge in total). The atomic trajectories after 10 ps of simulation show a sizeable region containing a large number of Sn atoms in addition to Ge atoms remaining crystalline. As such crystalline regions with significant amounts of Sn nucleate from the Sn_xGe_{1-x} melt even at 12.5% of germanium loading, the low rate of atomic diffusivity within the crystalline regions will strongly suppress the nucleation and growth of pure Ge phase-separated regions as we proposed above. It is important to note that the phase separation of Sn and Ge in Sn_xGe_{1-x} nanoalloys at *x* approaching unity is suppressed for a different reason. Fig 3b shows the atomic trajectories in the cell of 255 Sn atoms with 10 Ge atoms arranged in a compact cluster with the adamantane structure (4% Ge). Initially, Sn melts around Ge leaving the cluster intact (Fig 3b). However, between 10 and 15 ps (the period shown in Fig. 3c), the internal bonds of the cluster break, and cluster dissolves. Smaller Ge clusters were observed to dissolve even sooner. The growth of a separate Ge phase requires nucleation of a larger Ge cluster (over 10 atoms) that would bind Ge atoms faster than the atoms would diffuse into the melt. Although the occurrence of such large Ge clusters is very likely within a macroscopic volume of Sn_xGe_{1-x} alloy containing ~10^{23} atoms, they would form rarely within a particle of only ~10^3 atoms. Thus, we believe that the large size of the Ge critical nucleus makes it very unlikely that a separate Ge phase will nucleate within a Sn_xGe_{1-x} nanoparticle with large *x*. MD results are consistent with the proposed mechanism of alloy stabilization; further theoretical work towards deeper insights about the process are ongoing.

To inhibit phase separation at high temperature, we treated the NCs surface with sulfur, creating a thin layer of tin/germanium sulfides. The sulfur overcoating was carried out by introducing sulfur solution in oleylamine (S/OLA) into the Sn_xGe_{1-x} nanoparticle parent solution (See SI for experimental detail). The homogenous distribution of sulfur on the NCs surface is evidence by EDX elemental mapping images in Fig S8(b-e), which is further supported by X-ray photoelectron spectra showing a doublet from S $2p_{3/2}$ and $2p_{1/2}$ electrons in Fig S8(h). The sulfide coating does not have profound effect on optical properties of NCs, as the absorption spectra of NCs before and after sulfur overcoat appear nearly identical (Fig S9(a)) except for the slight blue shift of the latter as the effective size of Sn_xGe_{1-x} NCs is reduced upon the sulfur coating. The cubic structure of Sn_xGe_{1-x} NCs is entirely retained without reduction in tin content during the sulfur treatment as corroborated from XRD patterns [Fig S9(b)]

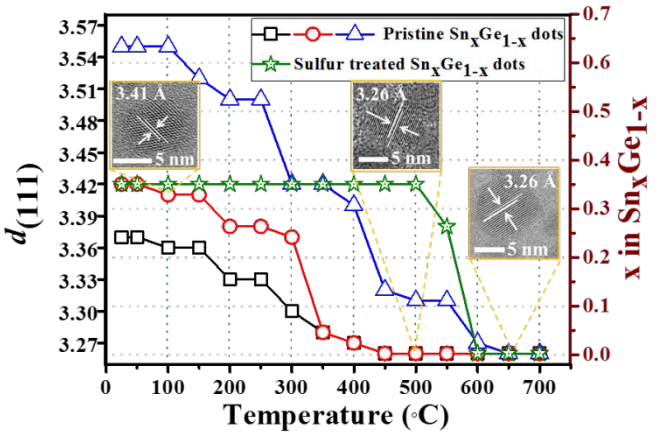

Fig 4. Values of d(111) from untreated Sn_xGe_{1-x} NCs with x = 0.25, 0.36 and 0.64, and sulfide-coated Sn_xGe_{1-x} NCs with x = 0.36 at different temperatures. Insets show TEM images of untreated Sn_xGe_{1-x} NCs at different temperatures. Samples were held for 10 min at each temperature.

To probe thermal stability, we chose to monitor the interatomic separation within the (111) plane of Sn_xGe_{1-x} alloy NCs by high temperature TEM as the NCs were heated up to 700 °C in 50 °C intervals (Fig. 4). Non-sulfidized NCs show a gradual decrease in d(111) value upon heating, indicative of slow diffusion of tin out of Sn_xGe_{1-x} lattice (Fig 4; insets show HRTEM images of particles before sulfur treatment at 100, 500 and 650 °C). On the contrary, the (111) lattice distance in sulfur-treated NCs does not change up to 500 °C, after which rapid phase separation was observed as manifested by the shrinkage of the distance to that of pure germanium (see further high-magnification HRTEM images in Fig S10). Importantly, due to the thin layer of Sn/Ge sulfides on the particle surface after the sulfur treatment, Sn_xGe_{1-x} NCs become amenable for ligand exchange process. Formerly soluble only in non-polar solvents, sulfur-treated particles become soluble in highly polar hydrazine or N-methylformamide. The replacement of long-chain insulating oleylamine molecules with small N_2H_4 or I^- allows close contacts among NCs in solution-cast films (Fig S9(c)-(d)), which can be expected to dramatically increase the charge carrier conductivity throughout the film.

In summary, we have developed a facile method for the synthesis of homogeneous Sn_xGe_{1-x} ($0 \le x \le 0.95$) alloy NCs with variable composition and size via the injection of a mixture of a Sn(II) amide and GeI_2 in alkylamine into the hot solution of *n*-BuLi in the amine. Mechanistic studies point to the initial formation of Sn-Ge cubane-like complexes that decompose into small β-Sn particles with chemisorbed Ge on the particle surface. They, in turn, convert to cubic Sn_xGe_{1-x} alloys upon diffusion of Ge into the particle interior at or above the melting temperature of tin. The synthesized NCs are thermally metastable and tin diffuses out of Sn_xGe_{1-x} nanoalloys at high temperatures, which can be mitigated by coating NCs with a thin layer of sulfur. In addition to improving the thermal stability, sulfur treatment also facilitates ligand exchange process with donor ligands on the surface of treated particles

Conflicts of interest

"There are no conflicts to declare".

J.M.P. acknowledges the support of the Center for Advanced Solar Photophysics, an Energy Frontier Research Center funded by the U.S. Department of Energy. K. R. was supported by a LANL LDRD funding. This work was performed, in part, at the Center for Integrated Nanotechnologies, an Office of Science User Facility operated for the U.S. Department of Energy (DOE) Office of Science. Los Alamos National Laboratory, an affirmative action equal opportunity employer, is operated by Los Alamos National Security, LLC, for the National Nuclear Security Administration of the U.S. Department of Energy under contract DE-AC52-06NA25396. Sandia is a multiprogram laboratory operated by Sandia Corporation, a Honeywell Company, for the US Department of Energy under contract DEAC04-94AL85000

Notes and references

1. M. A. Green, *J. Appl. Phys.* 1990, **67**, 2944.
2. H. Zimmermann, *Integrated Silicon Optoelectronics*, Springer Verlag Berlin Heidelberg, 2009.
3. H. Wu, N. Conrad, W. Luo, P. Ye, in *Electron Devices Meet. (IEDM), 2014 IEEE Int.*, 2014.
4. K. Wada, L. C. Kimerling, *Photonics and Electronics with Germanium*, Wiley- VCH, 2015.
5. J. Michel, J. Liu, L. C. Kimerling, *Nat. Photonics,* 2010, **4**, 527.
6. A. K. Okyay, D. Kuzum, S. Latif, D. A. B. Miller, K. C. Saraswat, *IEEE trans. Electron Devices,* 2007, ***54***, 3252–3259.
7. Z. Hu, S. Zhang, C. Zhang, G. Cui, *Coord. Chem. Rev.* 2016, **326**, 34–85.
8. S. Wu, C. Han, J. Iocozzia, M. Lu, R. Ge, R. Xu, Z. Lin, *Angew. Chemie - Int. Ed.* 2016, **55**, 7898–7922.
9. G. He, H. Atwater, *Phys. Rev. Lett.* 1997, 1937–1940.
10. H. P. Ladrón de Guevara, A. G. Rodŕiguez, H. Navarro-Contreras, M. A. Vidal, *Appl. Phys. Lett.* 2004, **84**, 4532–4534.
11. H. Lee, J. Cho, *Nano Lett.* 2007, **7**, 2638–2641.
12. S. Fan, L. Y. Lim, Y. Y. Tay, S. S. Pramana, X. Rui, M. K. Samani, Q. Yan, B. K. Tay, M. F. Toney, H. H. Hng, *J. Mater. Chem. A.* 2013, **1**, 14577.
13. M. G. Kim, J. Cho, *J. Electrochem. Soc.* **2009**, **156**, A277.
14. M. I. Bodnarchuk, K. V. Kravchyk, F. Krumeich, S. Wang, *ACS Nano* 2014, 2360–2368.
15. P. R. Abel, M. G. Fields, A. Heller, C. B. Mullins, *ACS Appl. Mater. Interfaces* 2014, **6**, 15860–15867.
16. Y. J. Cho, C. H. Kim, H. S. Im, Y. Myung, H. S. Kim, S. H. Back, Y. R. Lim, C. S. Jung, D. M. Jang, J. Park, et al., *Phys. Chem. Chem. Phys.* 2013, **15**, 11691.
17. S. Wirths, R. Geiger, N. V. Den Driesch, G. Mussler, T. Stoica, S. Mantl, Z. Ikonic, M. Luysberg, S. Chiussi, J. M. Hartmann, et al., *Nat. Photonics.* 2015, **9**, 88–92.
18. Y.-C.Y. Kain Lu Low, Y. Yang, G. Han, W. J. Fan, *ECS transcation* 2013, **50**, 519–526.
19. T. K. P. Luong, V. Le Thanh, A. Ghrib, M. El Kurdi, P. Boucaud, *Adv. Nat. Sci. Nanotechnol.* 2015, **6**, DOI 10.1088/2043-6262/6/1/015013.
20. M.-H. Lee, P.-L. Liu, Y.-A. Hong, Y.-T. Chou, Hong, Y.-J. Siao, *J. Appl. Phys.* 2013, **113**, 63517.
21. R. W. Olesinski, G. J. Abbaschian, *Bull. Alloy Phase Diagrams* 1984, **5**, 265–271.
22. O. Gurdal, P. Desjardins, J. R. A. Carlsson, N. Taylor, H. H. Radamson, J.-E. Sundgren, J. E. Greene, *J. Appl. Phys.* 1998, **83**, 162.
23. K. Ramasamy, P. G. Kotula, A. F. Fidler, M. T. Brumbach, J. M. Pietryga, S. A. Ivanov, *Chem. Mater* 2015, **27**, 4640.
24. R. J. A. Esteves, S. Hafiz, D. O. Demchenko, *Chem. Commun.* 2016, **52**, 11665.
25. R. J. A. Esteves, M. Q. Ho, I. U. Arachchige, *Chem. Mater* 2015, **27**, 1559.
26. S. A. Hafiz, R. J. A. Esteves, D. O. Demchenko, I. U. Arachchige, *J. Phys. Chem. Lett* 2016, **7**, 3295.
27. J. Barth, M. S. Seifner, J. Bernardi, *Chem. Commun.* 2015, **51**, 12282.
28. B. W. Boote, L. Men, H. P. Andaraarachchi, U. Bhattacharjee, J. W. Petrich, Javier Vela, E. A. Smith, *Chem. Mater*. 2017, **29**, 6012.
29. V. Tallapally, T. A. Nakagawara, D. O. Demchenko, U. Ozgur, I. U. Arachchige, *Nanoscale*, 2018, **10**, 20296.
30. P. Aella, C. Cook, J. Tolle, S. Zollner, A. V. G. Chizmeshya, J. Kouvetakis, *Appl. Phys. Lett.* 2004**, 84**, 888–890.
31. J. P. Hyung Soon Im, Y. Myung, K. Park, C. S. Jung, Y. R. Lim, *RSC Adv.* 2014, **4**, 15695.
32. M. S. Seifner, F. Biegger, A. Lugstein, J. Bernardi, S. Barth, *Chem. Mater* 2015, **27**, 6125.
33. M. S. Seifner, S. Hernandez, J. Bernardi, A. Romano-Rodriguez, S. Barth, *Chem. Mater* 2017, **29**, 9802.
34. M. Sistani, M. S. Seifner, M. G. Bartmann, J. Smoliner, A. Lugstein, S. Barth, *Nanoscale*, 2018, **10**, 19443.

Graphical Abstract

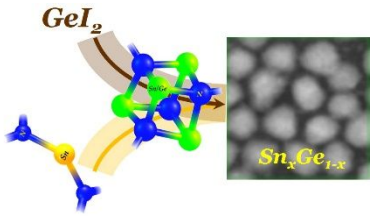

General synthetic route is reported leading to the cubic phase Sn_xGe_{1-x} alloy nanocrystals with composition varied from essentially pure Ge to 95% Sn. Overcoating of alloys with sulfide layer increases their thermal stability to 500 °C and also it makes the alloy nanocrystals amenable to easy ligand exchange the crucial step toward nanocrystal thin films with close interparticle contacts.